Atomic Spectroscopy

Article

Nitrogen-oxygen Co-doped Magnetic Micro-carbon Adsorbent Derived from Waste Toner Coupled with GFAAS for the Analysis of Trace Lead in Environmental and Biological Samples

Jie Song, Long Qin, Yue Dong, Chenchen Zhang, Yiwei Wu, and XiaoxiaoYu*

Hubei Collaborative Innovation Center for Rare Metal Chemistry, Hubei Key Laboratory of Pollutant Analysis & Reuse Technology, College of Chemistry and Chemical Engineering, Hubei Normal University, Huangshi 435002, P. R. China

Received: *September 03, 2023;* ***Revised:*** *October 14, 2023;* ***Accepted:*** *October 14, 2023;* ***Available online:*** *October 14, 2023.*

DOI: 10.46770/AS.2023.201

ABSTRACT: Currently, the social stock and scrappage of printers are both huge. The waste toner collected from the ink cartridges is difficult to degrade and has a small particle size, so the common treatment method is landfill, resulting in environmental pollution and resource wastage. This research aims to exploit the abundant presence of carbon black and magnetic powder in waste toner to synthesize nitrogen and oxygen co-doped magnetic carbon materials. It speculates that the amidation reaction between with the amino group of L-cysteine and the carboxylate group of waste toner in mild one-pot conditions leads to the incorporation of nitrogen and oxygen atoms. It significantly enhances the hydrophilicity of waste toner reducing the contact angle from 138.1° to 41.0° and provides active sites for the adsorption of Pb(II). Building upon this material, a novel approach combining magnetic solid-phase extraction with graphite furnace atomic absorption spectrometry has been developed for ultrasensitive lead analysis. This method demonstrates the detection limit of 43 ng L^{-1} with an RSD of 7.1% ($C_{Pb(II)}$ = 0.2 μg L^{-1}) and has been successfully employed for the analysis of trace lead in tap water, lake water, urine, and serum. Furthermore, this material exhibits rapid adsorption kinetics, robust resistance to matrix interferences, and low cost, thereby offering a novel avenue for mitigating environmental contamination through the concept of "waste-to-waste" treatment.

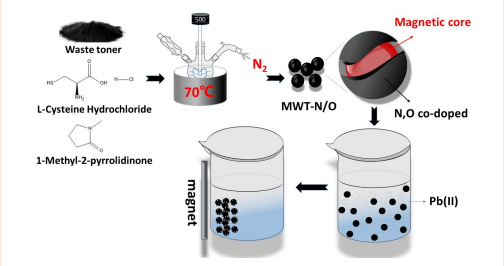

INTRODUCTION

As the era of globalized electronic information approaches, printers, as the most basic external output device of computers, are increasingly integrated into people's daily lives. The quantity of printers in use and the amount of waste generated are both enormous. It is estimated that by 2025, China will have 57 million discarded printers.[1] Toner cartridges are one of the main consumables of printers. Currently, in industry, only the aluminum materials in waste cartridges are recycled, [2] and there is no method for recycling the approximately 8% waste toner in the cartridges. The main components of waste toner are carbon black, magnetic powder, charge regulator, resin, and additives, including polypropylene resin-styrene copolymer (50-60%), Fe_3O_4 (20-30%), hydroxyaromatic acid and derivatives (10-20%), polyethylene/polypropylene wax (2−4%), and dispersant SiO_2 (1−3%).[3] The composition and performance of the toner change significantly after use, making it difficult to achieve recycling, even with regeneration treatment.[4] Therefore, the current primary methods of handling waste toner are incineration and landfill as municipal solid waste. However, due to the release of toxic gases at high temperatures.[5] and the difficulty of degradation and small particle size that can easily enter the human body,[6] landfilling is not a viable solution.[7] Currently, researchers have studied the potential applications of waste toner in different fields based on its properties, such as improving the performance of flocculants,[8] alumina films,[9] solar evaporation devices,[10] and oil-absorbing sponges [11] as additives. As a precursor, waste toner can be used to produce luminescent sensors (such as graphene quantum dots,[12] carbon quantum dots[13]) porous carbon materials (such as graphene oxide hydrogels,[14]) and magnetic functional materials (such as supercapacitors,[15] battery electrodes,[16] photocatalysts [17]),

providing ideas for the recycling and reuse of waste toner. However, waste toner generally contains carcinogenic organic compounds such as polycyclic aromatic hydrocarbons and dimethylnitrosamine, which can volatilize under high-temperature conditions. Therefore, although some of the aforementioned methods involving high-temperature treatments address the recycling and utilization of waste toner, the processing may lead to more severe environmental pollution.

Due to the rapid development of human industry, highly toxic heavy metals have seriously endangered environmental ecology, food safety, and human health through the amplification effect of the biological chain. Therefore, it is necessary to monitor the changes in heavy metal content in the environment and biological samples. Graphite furnace atomic absorption spectrometry (GFAAS) possesses advantages such as high sensitivity, low cost, small sample consumption, and simplicity, making it widely used for the detection of trace elements/elemental speciation in fields such as environmental monitoring, food analysis, and biological research. However, when directly applied to real sample analysis, challenges arise due to the interference from sample matrices that can affect the accurate determination of the instrument and the target element concentration being lower than the instrument's detection limit. Therefore, appropriate sample pretreatment techniques are often employed prior to GFAAS analysis to achieve the separation and removal of sample matrices and the enrichment of target analytes. Magnetic solid-phase extraction (MSPE) is a novel sample pretreatment technique based on magnetic solid-phase extraction materials. Compared to traditional solid-phase extraction techniques, MSPE simplifies the extraction process by utilizing magnetic extraction materials that can achieve rapid and simple phase separation under an external magnetic field. This eliminates the need for separate steps to separate and recover the extraction materials. Additionally, the magnetic extraction materials used in MSPE offer advantages such as a wide variety of options, ease of recycling and reuse, and reduced pretreatment costs. Therefore, it has been widely applied in the separation and enrichment of trace lead. For example, Hu's group utilized Fe_3O_4@SiO_2 as the magnetic core with zinc reagents [18] and Pb(II) imprinted polymers [19] on its surface. Some researchers The magnetic core surface has also been modified with aptamers that specifically recognize Pb(II), serving as highly selective adsorbents.[20] Montoro-Leal et al. modified graphene oxide nanospheres on the magnetic core surface to enhance the adsorption capacity for Pb(II).[21] A good MSPE generally has a large specific surface area, abundant pore structure with strongly acting functional groups for binding to heavy metal ions. At the same time, it requires easy recovery, physical and chemical stability, and low manufacturing cost. From the above requirements, waste toner has incomparable advantages: first, waste toner is a waste with extremely low cost [22] that urgently needs to be recycled; second, waste toner itself combines magnetic and carbon sources in one, and has the potential to become high-value carbon materials, eliminating the need for pre-preparation of magnetic cores and facilitating recovery. Furthermore, waste toner belongs to micro/nano materials and has certain adsorption sites. However, waste toner has strong hydrophobicity and is not conducive to the adsorption of heavy metals in aqueous solutions.

Here, this work intends to employ a mild and more environmentally friendly synthesis method to modify waste toner into carbon-based functional composite nanomaterials for reuse. N-methyl-2-pyrrolidone (NMP) has strong solubility and was used as the reaction solvent. L-cysteine, as a biologically essential amino acid, is green and environmentally friendly. It possesses functional groups such as amino, thiol, and carboxyl groups that are suitable for complexing heavy metal ions. Overall, in this project, nitrogen and oxygen atoms will be doped into waste toner through necessary functionalization in a one-pot system at a mild temperature and pressure to improve its hydrophilicity and the ability to adsorb heavy metals. The prepared MSPE agent will be combined with GFAAS for the detection of lead in environmental water and serum samples, realizing the environmental protection's concept of waste recycling.

EXPERIMENTAL

Materials and instruments. Detailed information was displayed in Supporting Information.

Preparation of nitrogen-oxygen co-doped magnetic micro-carbon adsorbent. The synthesis process flowchart for nitrogen-oxygen co-doped magnetic carbon material by a one-pot method is shown in Fig. 1. The specific steps are as follows: In a 100 mL round-bottom flask, 50 mL of NMP and 1.0 g of magnetic waste toner (MWT) were added. The flask was placed in an ultrasonic cleaner and sonicated until homogeneous. Then, 0.48 g of cysteamine hydrochloride and 0.030 g of azobisisobutyronitrile were added into the flask. The mixture was sonicated for 10 minutes while continuously flowing nitrogen gas. Simultaneously, stirring was performed at a speed of 500 r min^{-1}. The reaction was carried out under a water bath at 70°C for 7 hours. After completing the reaction, the heating apparatus was turned off, and stirring was maintained. The entire setup was allowed to cool naturally to room temperature. The product was subjected to solid-liquid separation using a neodymium-iron-boron magnet with the assistance of an external magnet. The resulting black precipitate sample was washed several times with ultrapure water until the supernatant becomes colorless and transparent. Finally, the thoroughly washed black precipitate sample was collected and dried in a vacuum oven at 30°C for a day. It was then ground for further use. The obtained material derived from waste toner is named MWT-N/O, where "N" and "O" indicate nitrogen and oxygen doping, as will be referred to later.

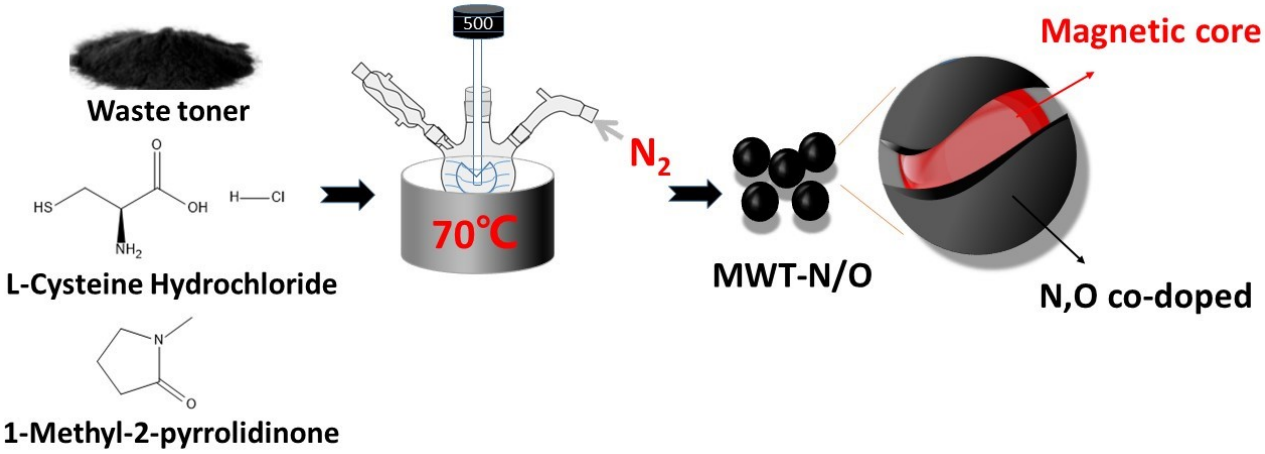

Fig. 1 Schematic diagram of MWT-N/O preparation.

MSPE process of MWT-N/O. Five mg of MWT-N/O was dispersed into10 mL solution containing an appropriate amount of Pb(II) (pH=6). The mixture was then sonicated for 2 min, and the MWT-N/O adsorbing Pb(II) was collected through magnetic separation. 0.2 mL of 0.1 mol L^{-1} HNO_3 was mixed with the solid material obtained in the previous step as an elution solution. After ultrasonic desorption for 15 min, the solid-phase material and elution solution were separated by magnetic separation, and the supernatant of the elution solution was collected. Finally, the content of Pb(II) in the desorption solution was measured by using GFAAS with the optimized operating parameters (Table S1).

Sample preparation. The certified environmental water standard (GSB 07-1183-2000, 20.3±2.4 μg L^{-1}) was provided by the China National Institute of Weights and Measures and used to validate the accuracy of our proposed method. Following the supplier's instructions, the ampoule was carefully broken, and 1 mL of GSB 07-1183-2000 was diluted 10-fold with ultrapure water in a 10 mL brown volumetric flask. The resulting certified sample was stored at 4 ℃ for future use. Tap water and Qingshan Lake samples were collected locally in Huangshi, Hubei, China. Urine and human blood serum samples were obtained from Huangshi Second Hospital (Hubei Province, China) with the approval of the local ethical committees, and the sample preparation process followed established protocols as described in the literature. [23] As indicated in Table S2, all actual samples were diluted with ultrapure water before analysis. During the MSPE procedure, take 10 mL of the aforementioned sample solution and adjust the pH to 6. Then, add 5 mg of MWT-N/O and perform ultrasonic extraction for 2 min. After magnetic separation, MWT-N/O adsorbing Pb(II) was collected, followed by the addition of 0.2 mL of 0.1 mol L^{-1} HNO_3 as an elution solution. The mixture was subjected to ultrasonic desorption for 15 min, and the supernatant of the elution solution was measured using GFAAS. Ultrapure deionized water was used as the blank control, and the obtained values were adjusted by subtracting the corresponding blank values to account for any background signals.

RESULTS AND DISCUSSION

Characterization of MWT-N/O. In order to understand the structural and morphological characteristics of MWT-N/O in detail, it was characterized by various technologies. Fig. 2a shows the thermogravimetric analysis (TGA) curve and the differential scanning calorimetry (DSC) curve of the pristine MWT, indicating that MWT undergoes significant thermal decomposition at 400°C, with a residual weight of 40% compared to its initial weight. Comparative analysis with information provided by the common toner suggests that MWT contains a substantial amount of thermally decomposable carbonaceous materials, namely, polystyrene, polyacrylic ester copolymers, and approximately 40% magnetic iron oxide. Fig. 2b displays the fourier transform infrared (FT-IR) spectra of MWT and MWT-N/O. It is observed that MWT-N/O has a simpler peak pattern compared to MWT, with a distinct absorption peak at 1630 cm^{-1} attributed to the vibration absorption of -CONH-.[24] At 570 cm^{-1}, both materials exhibit significant Fe-O peaks,[25] indicating the presence of magnetic iron oxide in both samples. Notably, the remaining characteristic peaks of MWT disappear (*e.g.* ester group and benzene ring), suggesting that not only doping reactions occurred during the synthesis process but also a portion of the polymer dissolved into the reaction solvent. Fig. 2c and 2d are the X-ray photoelectron spectroscopy (XPS) full spectra of MWT and MWT-N/O, respectively, revealing a significant increase in the nitrogen and oxygen content in MWT-N/O. Fig. 2e and 2f present the fine spectra of C 1s and N 1s for MWT-N/O. The peak at 285.54 eV is

Fig. 2 (a) TGA curve of MWT; (b) FT-IR spectra of MWT and MWT-N/O; XPS spectra for (c) MWT and (d) MWT-N/O (survey); the curve-fitting of XPS fine spectra of (e) C 1s, (f) N 1s for MWT-N/O.

attributed to C=O, while the peak at 285.03 eV is assigned to C-N [26], which corresponds to the C-N peak at 399.98 eV [27] in Fig. 2 (f). These characterization results of IR and XPS collectively indicate that amide bonds exist. Therefore, we speculate that the main component of MWT, polypropylene resin-styrene copolymer, undergoes hydrolysis in NMP solvent with weak alkalinity, resulting in the formation of alcohols and carboxylate salts. These carboxylate salts then undergo amidation reactions with the amino group of L-cysteine, leading to the incorporation of N and O into MWT-N/O during the synthesis process. We also conducted contact angle experiments before and after material modification. As shown in Fig. S1, the experimental results showed that the contact angle of the original MWT was 138.1°, indicating hydrophobicity. It is highly hydrophobic before treatment, cannot disperse in water. However, through this method, the doping of nitrogen and oxygen greatly enhances hydrophilicity. The contact angle of MWT-N/O decreased to 41.0°, enabling uniform dispersion in water and demonstrating potential for application as an adsorbent in aqueous solutions. Thus, MWT-N/O exhibited more hydrophilicity compared with MWT.

Figure 3a presents the scanning electron microscopy (SEM) image of MWT, while (b) shows the SEM image of MWT-N/O. By observing the morphological structure of MWT through SEM, it is found that the water bath reaction in this method removes the polymer that binds the magnetic particles on the surface of MWT, transitioning it from an agglomerated state to magnetic particle state of approximately 200 nm. This is in line with the significant weakening of peak intensities observed in the infrared spectra of MWT-N/O. By comparing with the reported particle size of iron oxide recovered from waste carbon powder in the literature,[28] it can be inferred that the magnetic core size is approximately 200 nm. Furthermore, from the comparison of magnetization curves of MWT and MWT-N/O in Fig. 3c, it can be observed that the magnetic saturation intensity of MWT-N/O increases from 35 emu g^{-1} to 88 emu g^{-1}, indicating a significant enhancement in magnetic strength. This further demonstrates that the dissolution of surface polymer during the reaction process significantly increases the proportion of iron oxide in the new material. XRD was also employed to characterize MWT and MWT-N/O, as shown in Fig.

Fig. 3 (a) SEM image of MWT; (b) SEM image of MWT-N/O; (c) Magnetization curves of MWT and MWT-N/O; (d) Zeta potential of MWT-N/O.

S2. By comparing the spectral peaks with the standard card JCPDS No. 75-0449 of Fe_3O_4, it was observed that the characteristic peaks of magnetite were maintained in both materials. To further elucidate the distribution of various elements on MWT-N/O, TEM images and element mapping were shown in Fig. S3. The results revealed that the magnetic iron oxide core is embedded within amorphous carbon, and there are overlapping regions where carbon, nitrogen, and oxygen elements coexist, confirming the speculation of amide formation. As shown in Fig. 3d, the zeta potential of MWT-N/O measured at pH=6 using a laser particle size analyzer is 2.16 mV.

Adsorption mechanisms. The adsorption percentages of the MWT-N/O for a mixed solution containing various metal ions at a concentration of 50 μg L^{-1} Ni(II), Co(II), Cd(II), Hg(II), Cu(II) and Pb(II) are shown in Fig. S4. The experimental results indicate that the adsorbent prepared in this study exhibits the highest adsorption percentages (~100%) for Pb(II), moderate adsorption capacity for Hg(II) and Cu(II), and almost no adsorption for Ni(II), Co(II) and Cd(II). As has been previously reported in the literature,[29] N-C=O plays a significant role in the Pb(II) adsorption. In addition, the bond energy between Pb(II) and hydroxyl groups of Fe oxides is proved to be more stronger than the other ions (Cd, Hg, Cu, Zn) in the reference.[30] Thus, the MWT-N/O sorbent presented the best adsorption performance for Pb(II) than other metal ions and Pb(II) were chosen as the target adsorbate for this MWT-N/O. Due to the positive zeta potential of the material, it is deduced that the adsorption of Pb(II) by the prepared MWT-N/O is not solely attributed to electrostatic adsorption but rather, it is largely attributed to the complexation of N and O dopant atoms with Pb(II). To demonstrate the mechanism of metal adsorption by MWT-N/O, we compared the Raman spectra of the material before and after Pb adsorption. As shown in Fig. S5, it revealed that MWT-N/O after adsorption of Pb(II) exhibited distinct characteristic peaks of Pb-O, indicating that Pb(II) primarily forms complexes with oxygen atoms on the MWT-N/O. The unshared electron pairs on the amino nitrogen of cysteine form a conjugated system with the π electrons of the carbonyl group, reducing the electron density on the nitrogen and weakening its proton accepting ability. Therefore, its ability to complex with Pb(II) is not as strong as that of oxygen atoms, which may be the reason why the Pb-N bond does not exhibit significant peaks in Raman spectra.

Optimization of MSPE.

(1) Effect of pH. The appropriate pH value is the vital factor affecting the adsorption process. Fig. 4 illustrates the influence of pH on the adsorption efficiency of Pb(II). It can be observed that the adsorption efficiency significantly increases from pH 3 to 6, and after pH 6, the adsorption efficiency exceeds 90%. It is speculated that the reason for this phenomenon is as follows: in a strongly acidic environment, hydrogen ions in the solution protonate the N atoms, increasing the positive charge of the adsorbent. This enhances the repulsion between MWT-N/O and Pb(II), thereby reducing the adsorption effectiveness. On the other hand, if the solution becomes highly alkaline, it may cause the formation of lead hydroxide precipitate. Therefore, a pH value of 6 was chosen for following experiments.

(2) Effect of sample volume and adsorption time. We then investigated the influence of sample volume (1−40 mL) on Pb(II) adsorption and the corresponding experimental data are presented in Fig. S6a. The findings revealed that even at a sample volume of 10 mL, a high adsorption rate (>90%) was maintained. As a result, 10 mL was chosen as the sample volume for all subsequent studies to achieve a higher enrichment factor. In addition, we examined the impact of ultrasonic adsorption time on the adsorption rate of Pb(II), varying the adsorption time from 1 to 30 min. The results, represented in Fig. S6b, indicated that the optimal adsorption effect was achieved at 1 min. Nonetheless, in consideration of the sample quantity and the requirement for manual shaking during sonication, a time of 2 min was employed in the subsequent experiments.

(3) Effect of elution conditions. As the concentration of hydrogen ions increases, the N atom undergoes protonation, resulting in an enhanced positive charge. This not only intensifies the repulsion between species with similar electrical properties but also reduces the coordination stability with Pb(II). As depicted in Fig. 4a of the preliminary pH optimization experiment, the reduction in pH has a notable impact on the adsorption rate. Consequently, we hypothesized that effective desorption of Pb(II) could be achieved by adjusting the acidic conditions. For this reason, HNO_3 was selected as the eluent, and a range of HNO_3 concentrations (0.05, 0.1, 0.2, 0.5 mol L^{-1}) was tested to investigate the elution of Pb(II). As displayed in Fig. S7, all the recoveries of Pb(II) met the requirements for quantitative elution when the nitric acid concentration exceeded 0.05 mol L^{-1}. Thereby, 0.1 mol L^{-1} HNO_3 was chosen as the concentration of eluent for subsequent experiments. Building upon this, we further investigated the influence of the volume of 0.1 mol L^{-1} HNO_3 as the eluent on the recovery of Pb(II). The data, shown in Fig. S8a, indicate that quantitative recovery of Pb(II) can be achieved with eluent volumes in the range of 0.2−2 mL. Since a smaller eluent volume leads to a better enrichment factor, a volume of 0.2 mL was selected to desorb Pb(II) in all subsequent experiments. Lastly, we further explored the influence of ultrasonic time for elution on the recovery of Pb(II). The results, shown in Fig. S8b, reveal a rapid increase in recovery rate within the range of 10 to 15 min. After 15 minutes, the material recovery rate remained consistently above 90% until complete elution was achieved. Theoretically, longer elution time leads to better elution effectiveness, but extended exposure to ultrasonic conditions may potentially deteriorate the surface structure of the material. Hence, it is advisable to avoid excessively long elution times. Consequently, a duration of 15 min was selected for the subsequent experiments.

Fig. 4 (a) Effect of pH on the adsorption percentage of Pb(II). (Conditions: 5 mg MWT-N/O; 1 mL sample volume containing with 50 μg L^{-1} Pb(II), sonicated for 30 min);(b) The pseudo-first-order kinetic plot and (c) pseudo-second-order kinetic plot for the adsorption of Pb(II) on MWT-N/O.

Coexisting ion interference. Under the optimized conditions mentioned above, a 10 mL solution with 2 μg L^{-1} Pb(II) was subjected to MSPE-GFAAS in the presence of various interfering ions , including K^+, Na^+, Ag^+, Ca^{2+}, Mg^{2+}, Zn^{2+}, Cu^{2+}, Cd^{2+}, Hg^{2+}, Co^{2+}, Ni^{2+}, Al^{3+}, Fe^{3+}, Cl^-, NO_3^-, SO_4^{2-}, PO_4^{3-}. This was done to assess the interference caused by coexisting ions. If the recovery rate of lead remains within the range of 85-115%, it indicates that the interference from the added coexisting ions can be considered negligible for the determination of the amount of Pb(II). Table S3 displays the maximum concentrations of the coexisting ions. When compared to the typical concentrations of common ions in environmental water, urine, and serum, this method exhibits strong resistance to interference from common ions. Hence, it is applicable for the detection of Pb(II) in actual environmental water samples and biological specimens.

Lifespan of MWT-N/O. The lifespan of the adsorbent is also a critical evaluation parameter. In this section of the experiment, the optimized extraction conditions mentioned earlier were employed. A fixed concentration of Pb(II) at 0.5 μg L^{-1} was used as the target for extraction. After completing one adsorption-elution experiment, the adsorbent was washed with approximately 10 mL of ultrapure water using ultrasound for about 30 s. The solution was then separated from the adsorbent using a magnet, and the supernatant was collected. This process was repeated two more times, and the collected supernatant was used for the next cycle of adsorption-elution experiments. The experimental results, as shown in the Fig. S9, indicate that MWT-N/O can be reused for at least 10 cycles.

Adsorption behavior. Five mg of adsorbent material was dispersed in a 5 mL solution with 50 mg L^{-1} Pb(II). The pH of the solution was adjusted to 6. This procedure was conducted in parallel for three experiments. The mixed solution was subjected to 24 h of adsorption with agitation. After magnetic separation, 2 mL of the supernatant was collected. The Pb(II) concentration in the supernatant was then quantified using flame atomic absorption spectroscopy. The adsorption capacity was found to be 15.6±0.09 mg g^{-1}. The adsorption rate of MWT-N/O for Pb(II) was investigated within a range of 1 to 60 min of adsorption time. As shown in the Fig. S10, it can be observed that MWT-N/O exhibits extremely rapid adsorption kinetics for Pb(II), reaching adsorption saturation within just 1 min. In addition, to elucidate the adsorption mechanism, the relevant data of adsorption kinetics were fitted to the pseudo-first-order and pseudo-second-order kinetic models. The results, as shown in Fig.4b and c, demonstrate that compared to the pseudo-first-order kinetic model, the pseudo-second-order kinetic model exhibits a better linear relationship (R^2=0.9994). Furthermore, the adsorption capacity of Pb(II) on MWT-N/O calculated based on the pseudo-second-order equation is 16.6 mg g^{-1}, which is very close to the experimental result of 15.6 mg g^{-1} obtained from the adsorption capacity experiment mentioned earlier. All of these data indicate that the adsorption behavior of Pb(II) on MWT-N/O follows the pseudo-second-order model, representing chemical adsorption behavior. Because the prepared MWT-N/O in this study also exhibits adsorption capacity for Hg(II) and Cu(II), to further evaluate the impact of Hg(II) and Cu(II) on the adsorption capacity of Pb(II), we separately investigated whether the presence of 50 mg L^{-1} Hg(II) and Cu(II) as coexisting interfering ions would affect the adsorption capacity of the material for 50 mg L^{-1} Pb(II). The results showed that the maximum adsorption capacity for Pb(II) was not significantly influenced, with values of 13.4 and 12.2 mg L^{-1} in the presence of Cu and Hg, respectively. It indicates a high selectivity of MWT-N/O for adsorbing Pb(II).

Analytical performance. The analytical performance of the MSPE-GFAAS method based on MWT-N/O was assessed using the optimized experimental conditions. The limit of detection (LOD), following the IUPAC definition as 3s/k, was determined to be 0.043 μg L^{-1}. Here, s represents the standard deviation of signal intensity obtained from nine replicate measurements of blank samples through the developed method, and k represents the slope of the calibration equation after preconcentration. The linear range extended from 0.15 to 3.0 μg $L^{-1}$with the linear equation derived as $y=0.6080C_x+0.0343$ (R^2=0.9979). The actual

Table 1. Comparison of other MSPE methods for the measurement of Pb(II) prior to GFAAS analysis

Sorbents	LOD (ng L^{-1})	Adsorption capacity (mg g^{-1})	Pretreatment time (min)	Reused times	Preparation condition	Refs.
Fe_3O_4@ Zincon@Si	10	21.5	2	3	Three-step synthesis >4h	18
MNPs@ DIP	9	150	10	10	Three-step synthesis >12h	19
Fe_3O_4@ Au@DNA	57	7.19	30	-	Five-step synthesis >24h	20
Fe_3O_4@graphene oxide	8	-	10	-	Three-step synthesis >24h	21
WT-500	3	31	7	5	One-pot calcine 500°C, 1h	25
MWT-N/O	43	16.6	17	>10	One-pot reaction 70°C, 7h,	This work

enrichment factor (EF), determined as the ratio of the slope of the calibration equation after and before MSPE, was determined to be was 51.6 that was consistent with the theoretical enrichment factor. The precision of the method, as indicated by the relative standard deviation (RSD), was found to be 7.1% at a Pb(II) concentration of 0.2 μg L^{-1}. This level of precision was confirmed through seven repetitive analyses, highlighting the method's excellent reproducibility.

The present method was compared with previously reported MSPE-GFAAS methods, and the comparative results are listed in Table 1. It can be observed that the LOD and the analysis time of the developed method as well as the adsorption capacity of the prepared MWT-N/O are at an intermediate level. Although the method described in reference 18 has an obvious shorter reaction time, it requires drying of the magnetic beads in between steps, and the repeated usage of the zinc reagent is limited due to its tendency to detach during ultrasound processes. Compared to the reported works, the prominent advantage of this study is the simplicity of the synthesis steps. Due to the inherent advantages of waste toner as both a carbon material and a magnetic material, a simple one-pot synthesis approach can be employed. In contrast, other works require at least three or more steps for pre-synthesizing magnetic cores as described in references.[18-21] Additionally, due to the mild desorption conditions required for this material, with a low concentration of 0.1 mol L^{-1} HNO_3, the structure of this material can maintain its adsorption capacity during the desorption process, resulting in sustained efficacy. Even after ten repeated uses, a high recovery rate can still be maintained. Furthermore, compared to our previous high-temperature carbonization method,[25] the reaction temperature is lower, which helps to avoid the generation of harmful gases, making it more environmentally friendly.

Applications. To validate the accuracy of our proposed method, it was applied to the analysis of the GSB 07-1183-2000 environmental water standard (20.3±2.4 μg L^{-1}). The detection values obtained (21.1±0.9 μg L^{-1}) by the method were compared to the standard reference values using the t-test to assess if there were significant differences between them. The computed t-value (2.02) was less than the critical t-value ($t_{0.05,4}$=2.78), indicating a good agreement between the measured values obtained by the method and the standard reference values. This confirms that the method exhibits good accuracy.

Table 2 Analytical results (mean ± SD, n=3) of Pb(II) in real water and biological samples

Sample	Added (μg L^{-1})	Found (μg L^{-1})	Recovery (%)
Tap water	-	7.54 ± 0.05	-
	10.0	16.4 ± 0.01	96.8
	20.0	25.5 ± 0.06	93.0
Qingshan lake	-	19.5 ± 0.005	-
	10.0	29.9 ± 0.03	104
	20.0	38.9 ± 0.03	97.2
Blood serum	-	34.2 ± 0.02	-
	40.0	70.9 ± 0.05	91.7
	80.0	110 ± 0.1	95.7
Urine	-	48.7 ± 0.02	-
	20.0	68.9 ± 0.1	101
	40.0	88.3 ± 0.1	98.9

The established MSPE-GFAAS method was applied to the determination of Pb(II) in tap water, Qingshan lake, human urine and human serum. The four types of samples mentioned above were subjected to dilution treatment and directly used for analysis. Different levels of Pb(II) were detected in all samples, followed by a spike recovery experiment. As shown in Table 2, the obtained Pb(II) spike recovery rates ranged from 91.7% to 104%. These results demonstrate that the proposed method exhibits good accuracy for the analysis of the amount of Pb(II) in real environmental water and biological samples.

CONCLUSIONS

This work utilized waste toner powder and cysteamine hydrochloride as reaction materials to prepare nitrogen-oxygen co-doped magnetic micro-carbon adsorbent, using a mild one-pot synthesis approach. Compared to the original MWT, MWT-N/O exhibited hydrophilicity and the ability to adsorb heavy metals due to the incorporation of nitrogen and oxygen heteroatoms. Based on this material, a new method combining MSPE and GFAAS was proposed for the analysis of Pb(II) in environmental water and biological samples. This magnetic solid-phase extraction sorbent derived from waste toner not only demonstrated strong resistance to matrix interference and rapid adsorption kinetics but also had positive practical significance in terms of reducing the cost of the magnetic solid-phase adsorbent and minimizing pollution from waste toner. This approach provides a new perspective for the treatment of environmental pollution following the concept of "using waste to treat waste."

ASSOCIATED CONTENT

The supporting information (Figs. S1−S10 & Tables S1−S3) is available at www.at-spectrose.com/as/home.

AUTHOR INFORMATION

Xiaoxiao Yu received her BS degree in Applied Chemistry from Huazhong Agricultural University and PhD degree in Analytical Chemistry from Wuhan University in 2015 and 2020, respectively. From June 2020 to present, she worked as a Lecturer at College of Chemistry and Chemical Engineering of Hubei Normal University. Her major research interests include the development and application of advanced materials for environmental, food and biological analysis. She is author or co-author of over 15 articles published in peer-reviewed scientific journals and authorized 2 Chinese invention patents.

Corresponding Author

* X. X. Yu

Email address: yuxiaoxiao@hbnu.edu.cn

Notes

The authors declare no competing financial interest.

ACKNOWLEDGMENTS

This work was supported by Natural Science Foundation of Hubei Province of China (2022CFD038).

REFERENCES

1. Q. B. Song, J. H. Li, L. L. Liu, Q. Y. Dong, J. Yang, Y. Y. Liang, and C. Zhang, *J. Clean Prod.*, 2016, **112**, 4461–4468. https://doi.org/10.1016/j.jclepro.2015.07.106
2. J. J. Ruan and Z. M. Xu, *Environ. Sci. Technol.*, 2012, **46**, 6214–6221. https://doi.org/10.1021/es3008358
3. J. J. Ruan, J. Li, and Z. M. Xu, *J. Hazard. Mater.*, 2011, **185**, 696–702. https://doi.org/10.1016/j.jhazmat.2010.09.074
4. T. G. Gutowski, S. Sahni, A. Boustani, and Graves. S. C, *Environ. Sci. Technol.*, 2011, **45**, 4540–4547. https://doi.org/10.1021/es102598b
5. A. A. Vucinic, D. Vujevic, K. Mujkic, and M. Novak, *Chem. Eng. Trans.*, 2013, **34**, 121–126. https://doi.org/10.3303/cet1334021
6. J. J. Ruan, B. J. Qin, and J. X. Huang, *Environ. Int.*, 2018, **118**, 92−96. https://doi.org/10.1016/j.envint.2018.05.038
7. J. W. Gu, S. Karrasch, and T. Salthammer, *Indoor Air*, 2020, **30**, 396−421. https://doi.org/10.1111/ina.12646
8. M. A. Notani and M. Mokhtarnejad, *Proc. Inst. Civ. Eng.-Co.*, 2020, **173**, 123−131. https://doi.org/10.1680/jcoma.17.00072
9. P. Nezhadi, M. Azadi, and M. S. Bahaabad, *Surf. Interfaces*, 2020, **18**, 11. https://doi.org/10.1016/j.surfin.2020.100450
10. M. N. A. Ivan, A. M. Saleque, S. Ahmed, Cheng, P. K. Cheng, J. P. Qiao, T. I. Alam, and H. T. Yuen, *ACS Appl. Mater. Interfaces*, 2022, **14**, 7936−7948. https://doi.org/10.1021/acsami.1c22215
11. P. Shi, Y. T. Wang, X. K. Hu, M. Duan, and X. J. Wang, *J. Hazard. Mater.*, 2018, **360**, 615−622. https://doi.org/10.1016/j.jhazmat.2018.08.052
12. Q. Xu, Y. Gong, Z. F. Zhang, Y. M. Miao, D. X. Li, and G. Q. Yan, *Microchim. Acta*, 2019, **186**, 483. https://doi.org/10.1007/s00604-019-3539-x
13. H. F. Gao, L. K. Wen, Y. H. Wu, Z. F. Fu, and G. Wu, *Biosens. Bioelectron.*, 2017, **97**, 122−127. https://doi.org/10.1016/j.bios.2017.04.033
14. Z. S. Tian, K. S. Cao, S. Z. Bai, G.X. He, and J. T. Li, *ACS Sustain. Chem. Eng.*, 2019, **7**, 496−501. https://doi.org/10.1021/acssuschemeng.8b03997
15. S. Kaipannan, K. Govindarajan, S. Sundaramoorthy, and S. Marappan, *ACS Omega*, 2019, **4**, 15798−15805. https://doi.org/10.1021/acsomega.9b01337
16. Y. Li, Mao, J. Q. Xie and H. Q. Li, and J, J. Mater. *Cycles Waste Manag.*, 2018, **20**, 361−368. https://doi.org/10.1007/s10163-017-0599-z
17. Y. R. Fan, X. Wang, X. T. Guo, H. J. Pan, Y. Q. Xing, Y. L. He, Y. P. Yuan, L. L. Zhang, Y. Y. Song, Y. M. Liu, and S. G. Shen, *New J. Chem.*, 2023, **47**, 5229−5237. https://doi.org/10.1039/d3nj00298e
18. H. M. Jiang, Z. P. Yan, Y. Zhao, X. Hu, and H. Z. Lian, *Talanta*, 2012, **94**, 251−256. https://doi.org/10.1016/j.talanta.2012.03.035
19. B. S. Zhao, M. He, B. B. Chen, and B. Hu, *Microchim. Acta*, 2019, **186**, 775. https://doi.org/10.1007/s00604-019-3819-5
20. Y. K. Li, W. T. Li, X. Liu, T. Yang, M. L. Chen, and J. H Wang, *Talanta*, 2019, **203**, 210−219. https://doi.org/10.1016/j.talanta.2019.05.075
21. P. Montoro-Leal, J. C. Garcia-Mesa, M. T. Siles Cordero, M. M. Lopez Guerrero, and E. Vereda Alonso, *Microchem. J.*, 2020, **155**, 10476. https://doi.org/10.1016/j.microc.2020.104796
22. S. Joseph, G. Saianand, M. R. Benzigar, K. Ramadass, G. Singh, A. I. Gopalan, H. Y. Jae, T. Mori, A. H. Al-Muhtaseb, J. B. Yi, and A. Vinu, *Adv. Sustain. Syst.*, 2021, **5**, 2000169. https://doi.org/10.1002/adsu.202000169
23. Y. N. Yang, H. Wang, Y. W. Wu, and X. X. Yu, *Spectrochim. Acta A*, 2022, **265**, 120385. https://doi.org/10.1016/j.saa.2021.120385
24. D. Luo, S. G. Liu, N. B. Li, and H. Q. Luo, *Microchim. Acta*, 2018, **185**, 284. https://doi.org/10.1007/s00604-018-2817-3
25. X. X. Yu, C. X. Zhu, H. Wang, and Y. W. Wu, *Anal. Bioanal. Chem.*, 2022, **414**, 2409−2418. https://doi.org/10.1007/s00216-022-03879-x
26. Y. B. Yan, J. Chen, N. Li, J. Q. Tian, K. X. Li, J. Z. Jiang, J. Y. Liu, Q. H. Tian, and P. Chen, *ACS Nano*, 2018, **12**, 3523−3532. https://doi.org/10.1021/acsnano.8b00498
27. D. H. Kim and T. W. Kim, *Nano Energy*, 2018, **51**, 199−205. https://doi.org/10.1016/j.nanoen.2018.06.064

28. J. J. Ruan, L. P. Dong, J. X. Huang, Z. Huang, K. Huang, H. L. Dong, T. Zhang and R. L. Qiu, *ACS Sustain. Chem. Eng.*, 2017, **5**, 4923–4929. https://doi.org/10.1021/acssuschemeng.7b00328
29. J. Q. Deng, Y. Q. Liu, S. B. Liu, G. M. Zeng, X. F. Tan, B. Y. Huang, X. J. Tang, S. F. Wang, Q. Hua, and Z. L. Yan, *J. Colloid Interface Sci.*, 2017, **506**, 355–364. https://doi.org/10.1016/j.jcis.2017.07.069
30. S. S. Li, M. Jiang, T. J Jiang, J. H. Liu, Z. Guo, and X. J. Huang, *J. Hazard. Mater.*, 2017, **338**, 1–10. https://doi.org/10.1016/j.jhazmat.2017.05.017